

# Tidal flood area mapping fronts the climate change scenarios: case study in a tropical estuary of Brazilian semiarid region

Paulo Victor N. Araújo<sup>1,2,3</sup>, Venerando E. Amaro<sup>1,3</sup>, Leonlene S. Aguiar<sup>3</sup>, Caio C. Lima<sup>3,4</sup>, and Alexandre B. Lopes<sup>5</sup>

5 <sup>1</sup>Postgraduate Program in Geodynamics and Geophysics (PPGG), Federal University of Rio Grande do Norte, P.O. Box 1524, Natal-RN, 59078-970, Brazil

<sup>2</sup>Research Group on Environmental Analysis, Modelling and Geoinformation (PAMGEIA), Federal Institute of Education, Science and Technology of Rio Grande do Norte, Macau-RN, 59500-000, Brazil

10 <sup>3</sup>Laboratory of Geotechnologies, Coastal and Ocean Modelling (GNOMO), Department of Civil Engineering, Federal University of Rio Grande do Norte, Natal-RN, 59078-970, Brazil

<sup>4</sup>Federal Institute of Education, Science and Technology of Rio Grande do Norte, Natal-RN, 59015-000, Brazil

<sup>5</sup>Center of Sea Studies, Federal University of Parana, P.O. Box 61, Curitiba-PR, 83225-976, Brazil

*Correspondence to:* Paulo Victor N. Araújo (paulo.araujo@ifrn.edu.br)

15 **Abstract.** Previous studies on tidal flood mapping are mostly with continental and/or global scale approaches. Besides, the few works on local scale perception are concentrated in Europe, Asia, and North America. Here we present a case study approaching a tidal flood risk mapping methodology against climate change scenarios in a region with a strong environmental and social appeal. The study site is an estuarine cut in the Brazilian semi-arid, covering part of two state conservation units, which has been in recent years suffering severe consequences from tidal flooding. In this case study, high geodetic precision  
20 data (LiDAR DEM), together with robust tidal return period statistics and data from current sea level rise scenarios were used. We found that approximately 327.60 km<sup>2</sup> of the estuary is under tidal flood risk area. in need of mitigation measures. This case study can serve as a basis for future management actions as well as a model for applying risk mapping in other coastal areas.

## 1 Introduction

Climate change has been associated with various environmental and socioeconomic damages worldwide, with global mean  
25 sea level rise (SLR) being one of the main associated phenomena (Nicholls and Cazenave, 2010; IPCC, 2014; Busman et al., 2016; Dangendorf et al., 2019; Bamber et al., 2019). The SLR global mean is occurring at an accelerating rate, averaging about +3 mm/year (recorded for during the last quarter-century), threatening coastal communities and ecosystems worldwide (Nerem et al., 2018; Bamber et al., 2019). SLR will radically redefine the coastline of the 21st century (Taherkhani et al., 2020).

The changes produced by rising and falling the mean sea levels have important implications for the dynamics and morphology  
30 of coastal environments, and it is in these environments that a considerable part of the world's population lives (Neumann et al., 2015). Besides, it has been causing flooding of natural habitats and coastal infrastructures and consequently causing environmental and socioeconomic impacts of varying magnitude (Dwarakisha et al., 2009; IPCC, 2014; Murray et al., 2019).

Decades ago, the flooding usually happened only during a powerful or localized storm now can happen when a steady breeze or a change in coastal current overlaps with high tide, as occurs for example in USA (NOAA, 2019).

35 In decades past, high tide flooding had little impact on coastal communities because our shorelines were not as heavily developed, and sea level was not as high. Today, however, the reach and effect of the tides is changing, and many coastal towns and cities are already grappling with how best to protect their communities and infrastructure (Dahl et al., 2017).

In Brazil, the current panorama of coastal flooding is worrying. The Brazilian Panel on Climate Change (PBMC) systematized data and information indicating that the different regions of Brazil are already experiencing changes in their characteristic  
40 climates (PBMC, 2014). These changes are expected to affect the country's natural, human, infrastructure and production systems in a non-uniform manner (Brasil, 2016). The country stands out as the seventh largest nation in the world by coastal population and the seventh largest proportion of the coastal zone in the low-lying area (Mcgranahan et al., 2007). About 25% of the Brazilian population lives in the coastal zone and has lately been suffering from the damage caused by the relative rise in sea level (SMC-Brasil, 2018). Approximately 60% of the natural events that hit Brazil from 1948 to 2006 with harmful  
45 consequences to the population were related to flooding and/or sea advances (Brasil, 2016). These data, combined with scenarios of rising sea level trends (Easterling et al., 2000; Taherkhani et al., 2020), warn of the need for (local scale) projections for the next decades, to support the preparation and planning to respond to increasing threat related to sea level rise. According to Taherkhani et al., 2020, the 21st century will see significant changes to coastal flooding regimes (where present-day, extreme-but-rare events become common), which poses a major risk to the safety and sustainability of coastal  
50 communities worldwide. Climate risk adaptations involving large infrastructure investments represent difficult decisions and require an accurate information base (Hall et al., 2019; Kulp and Strauss, 2019).

Coastal flooding is becoming more frequent and expensive with sea level rise (SLR) (Herdman et al., 2018). Dahl et al. (2017) concluded that sea level rise drives increased tidal flooding frequency at tide gauges along the U.S. East and Gulf Coasts in projections for next years. The 5th report of the Intergovernmental Panel on Climate Change (IPCC) presented climate  
55 scenarios called Representative Concentration Pathway (RCP) (IPCC, 2014). Each RCP was built for the global scale and considers for the projection of relative elevation of MSL the historical evolution of several factors, such as gas emission, the concentration of effect gases, among others. Although in all scenarios the projected increase in MSL is a maximum of 1m for the year 2100, they have been prepared for global and continental scale. Many studies have analysed the risk arising from these flood scenarios across the low-lying coastal zone (altitude up to 10m) (Nicholls et al., 2007; Dwarakish et al., 2009; Nicholls  
60 and Cazenave, 2010; Nicholls et al., 2011; Boori et al., 2012; Busman et al., 2016). However, the lack of work on the theme in focus in the South American region and especially in Brazil is striking. Therefore, the objective of this work was develop and apply a methodology for tidal flood risk mapping, given the current scenarios of rising sea level trends, adopting as a case study the Piranhas-Açú Estuary, the northern portion of the state of Rio Grande do Norte, Brazil.

## 2 Study area

65 The tropical watershed of the Piancó-Piranhas-Açu River is located in northeastern Brazil and is the largest basin of the  
Northeast East Atlantic Hydrographic Region, with a total area of 43,683 km<sup>2</sup>. Its territory is divided between the states of  
Paraíba (60%) and Rio Grande do Norte (40%). Fully inserted in very hot and semi-arid climate territory, the basin presents  
concentrated rainfall in a few months of the year (rainy late to autumn) and a pattern of strong interannual variability,  
70 characterized by alternation between years of above average, regular and consecutive years of below-average values resulting  
in prolonged droughts and low water availability.

The study area covers the entire Piancó-Piranhas-Açu estuary, represented by a rectangle in the measurements 62 x 35.5 km,  
corresponding to an area of approximately 2,201 km<sup>2</sup>. This area is an estuarine section comprising parts of 4 municipalities of  
the northern coast of the state of Rio Grande do Norte (Porto do Mangue, Carnaubais, Pendências, and Macau) (Figure 1).

In general, the area under study is represented by a Tropical of Equatorial Zone climate, and framed in the semiarid climate  
75 subdomain (Diniz and Pereira, 2015).. The region in focus stands out as the driest stretch of the entire Brazilian coast, with an  
average rainfall of 537.6 mm/year in Macau City. The daily temperatures vary from 26°C to 30°C (with a mean temperature  
of 26.8°C), and the average relative air humidity is 70% (IDEMA, 1999; Diniz and Pereira, 2015; Barbosa et al., 2018a). In  
geomorphological terms, there is a wide fluvial-marine plain that constitutes the Coastal Strip (Barbosa et al., 2018b, Costa et  
al., 2020). The number and extent of various channels present along adjacent large river plains reveal the great influence of  
80 oceanic waters on this stretch of the continent, with tidal action being one of the major natural forces responsible for  
hydrographic control.

The study area is inserted in sheltered coastal region dominated by tide-modified to tide-dominated beaches. (Vital et al., 2016).  
In this region, the local tide is semidiurnal, with two high and two low tides, where the average level set as a reference is 1.39  
m above the reduction level (RL), as established by the Hydrography and Navigation Directorate (DHN) of the Brazilian Navy  
85 (MB). The DHN of MB, the body responsible for maritime monitoring, adopts the so-called reduction level (RL) as a reference  
for maritime quota. The RL is level that corresponds to the average of low tides of syzygy, to eliminate the variations of tides  
and to guarantee to navigator that it does not find any depth less than those represented in the nautical chart. In region, It has  
mean semidiurnal high tides of 2.34 m above reduction level, mean quadrature of high tides of 2.21 m, average low tide of  
0.43 m of tidal seas below mean level of squared low seas of 0.56 m (Matos et al., 2019; DHN, 2018). As for the marine  
90 currents, the region is under the influence of the Southern Equatorial Current that acts throughout the northern coast of Brazil  
(Diniz et al, 2017).

In general terms, this coastal region has a mosaic of ecosystems marked by mangrove forests, together with extensive ebb tidal  
delta, exposed and sheltered sandy ocean beaches, barrier island systems, active dune fields, spits and short-term high-  
sedimentary dynamic tidal channels (Grigio et al., 2006; Amaro et al., 2012; Santos and Amaro, 2013; Busman, et al., 2016;  
95 Vital et al., 2016). The industrial sector of the area under study comprises essentially mineral exploration, especially salt, oil,  
and gas. The extraction of oil and natural gas is a very important activity in the basin and economy of the state of Rio Grande

do Norte, due to the royalties generated (IDEMA, 2005). Aquaculture and artisanal fishing also play a part in the local economy, as well as irrigated agriculture, shrimp farming, salt marshes and, more recently, typical wind industry infrastructure. There are two noteworthy state conservation units in the study area: Ponta do Tubarão State Sustainable Development Reserve (RDSEPT) and the Rosado Dunes Environmental Protection Area (APADR). RDSEPT was created through State Law No. 8.349 of July 18, 2003, and its objectives are to safeguard the traditional way of life, to ensure activities based on sustainable exploitation of natural resources, traditionally developed over generations and adapted to local ecological conditions and which play a fundamental role in protecting nature and maintaining biological diversity. APADR was recently created by State Decree No. 27,695 of February 21, 2018, and aims to protect biological diversity, discipline the occupation process and ensure the sustainable use of the natural resources of the respective area.

Historically, although the Piranhas-Açú Estuary has suffered from some drastic river flooding in the last decade (2004, 2008 and 2009) as a result of extreme rainfall events (Medeiros and Zanella, 2019; Medeiros, 2019), it has been suffering lately with the effects of tidal flooding (type of focus flooding of this job). Recent reports, from the years 2010, were found in local newspapers and blogs, as well as personal observation in loco (personal communication). Since then, frequently, due to the effects of the sea, streets and houses are invaded by water, bringing negative consequences to several communities of the northern coast of Rio Grande do Norte (Figure 2). The current facts, allied to the local disordered occupation, the environmental and economic importance of the region, the scenarios of sea level rise, and finally, the lack of literature on the case (tidal flood), make this region an area of great appeal for the development of scientific works, to subsidize information for decision-making on climate change adaptations.

### 115 **3 Material and methods**

Tidal flood risk mapping was performed using data on the meteorological tide, astronomical tide and a high-resolution LiDAR Digital Elevation Model (DEM), both calibrated for the study area. Data were subjected to statistical analysis and return period calculations. The 20-year return period was adopted as the base reference quota for this study and allied with the projections found in the literature on the global sea level rise for the coming years. Finally, flood risk mapping was performed based on flood scenarios and the vulnerability of land use and cover.

#### **3.1 Tide database**

For this study, sea level variation was represented by the sum of the meteorological and astronomical tide (SMC-Brasil, 2018).

##### **3.1.1 Meteorological tide (MT)**

The MT or storm surge (also known as non-astronomical sea level) is the result of atmospheric forcing such as wind pressure or sea level pressure variations. To compose the local MT historical series, the maximum annual tide level was obtained from the data from point 19 (Lat. 4,821 ° W / Long. 36,500 ° S) (Figure 1) from the GOS (Global Ocean Surge) database of the

SMC-Brasil project (SMC-Brasil, 2018). This database is a selection of regional reanalysis series, located along the Brazilian coast, built with a forced numerical simulation with atmospheric pressure fields and winds and validated for the region. To generate the series, the barotropic module (2DH) of the model in global mesh with  $0.25^\circ$  spatial resolution and bathymetry data of ETOPO2 model (NOAA) was used. As forcing the model, pressure data at sea level and global winds (10m high) from Reanalysis 1 (NCEP / NCAR) were used. The wind and pressure data have a spatial resolution of  $1.9^\circ$  and a 6-hour temporal resolution. Each of the series has a duration of 60 years (1948-2008) with a time interval of 1 hour (SMC-Brasil, 2018).

### 3.1.2 Astronomical tide (AT)

The AT is defined as the set of regular sea level rise and fall motions over 12 or 24 hours, produced by the gravitational effects of the Earth-Moon-Sun system. Other celestial bodies in the solar system are also attractive, yet small when compared to and considered by the moon and sun. Tide description and prediction at a given location can be done by harmonic tidal analysis (Pugh, 1987). For this job, the Astronomical Tide data are the result of deterministic forecasts prepared and provided by the Brazilian Navy's Directorate of Hydrography and Navigation (DHN). The maximum annual astronomical tide level was used from the astronomical tide forecast data released by DHN, linked to the Port of Macau tidal gauge station (Lat.  $4^\circ 49' 05''$ S / Long  $37^\circ 02' 04''$  W) (Figure 1), for the period 1998 to 2018. These data were available through tables showing the maximum and minimum daily values of astronomical tidal heights.

### 3.1.3 Statistical analyses of tide database

The Mann–Kendall sequential test (Mann, 1945; Kendall, 1975) was applied to evaluate the temporal serial behaviour of annual maximum of meteorological tide and astronomical tide. The Mann–Kendall test is a robust, sequential, and non-parametric statistical method used to determine if a specific data series has a temporal tendency towards statistically significant changes. Among its advantages, it does not require normal distribution of data and is only slightly influenced by abrupt changes or non-homogenous series (Zhang et al., 2009). In recent years, with growing concerns over environmental degradation and about the implications of greenhouse gases on the environment, researchers and practitioners have frequently applied the non-parametric Mann–Kendall test to detect trends in recorded hydrologic time series such as water quality, streamflow, and precipitation time series (Yue and Wang, 2004; Araújo et al., 2019). Although it has no influence on the tidal flood risk mapping, the Mann–Kendall test was applied to investigate if the elevation of tides is showing any upward or downward trend. Then, the data was submitted for fit extreme value of gumbel distribution function (Gumbel, 1958). Extreme value statistics are used primarily to quantify the stochastic behaviour of a process at unusually large (or small) values. Particularly, such analyses usually require estimation of the probability of events that are more extreme than any previously observed. Many fields have begun to use extreme value theory, and some have been using it for a very long-time including meteorology, hydrology, finance and ocean wave modelling to name just a few (Gilleland and Katz, 2016). The Gumbel Distribution also is known as Type I extreme value distribution, or Fisher-Tippet type I distribution, has the function of accumulated probabilities given by the equation, Eq. (1):

$$F_X(x) = P\{X < x\} = e^{-e^{-y}}, \quad (1)$$

160 Being  $x$  the ratio  $y$  a reduced variable Gumbel given by, Eq. (2):

$$y = \frac{x-\beta}{\alpha}, \quad (2)$$

Where  $\alpha$  and  $\beta$  are characteristic parameters of the Gumbel line;  $\alpha$  represents meter of scale and  $\beta$  the position parameter. The return period ( $Tr$ ) in years can be obtained by the equation, Eq. (3):

$$x(Tr) = \beta - \alpha \ln \left[ -\ln \left( 1 - \frac{1}{Tr} \right) \right], \quad (3)$$

165 In this work, the 20-year return period ( $Tr_{20}$ ) was adopted as the starting reference for flood hazard mapping at present. All statistical analyses were performed using R software (R Development Core Team, 2020). The packages used were “Kendall” and “extRemes”, for Mann – Kendall sequential test and fit extreme value of Gumbel distribution function, respectively.

### 3.2 Adjustment of Reduction Level to the Brazilian Geodetic System

170 The astronomical tidal information provided by DHN is all linked to the so-called Reduction Level (RL), which is the altimetric reference system for bathymetric depth measurement adopted by the Brazilian Navy (MB). This reference system assigns the average low tides of spring to a measurement reference made at the local level. Thus, the establishment of the local sea level found in the nautical charts and information provided by the Brazilian Navy has its own framework aimed at knowledge of the seabed relief for navigators' safety (CHM, 2019a, 2019b). Therefore, it is a different altimetric reference than the official geodetic reference system adopted by the country (Matos, 2005; Ramos & Krueger, 2009).

175 Therefore, to standardize the altimetric reference of this work, Imbituba's Datum Vertical was adopted, linked to the Brazilian Geodetic System (SGB). For this purpose, a level reference point was traced over approximately 50 minutes employing a two-frequency GNSS receiver (L1 / L2) near the port of Macau (Figure 3). This landmark, codenamed RN-2 (DHN), was deployed during the construction of the respective navigational station by the Brazilian Navy. After the screening, the GNSS data were submitted to coordinate adjustment post-processing to the MAPGEO2015 geoidal model and obtained its SGB-linked  
180 orthometric altitude, through the Precise Point Positioning of the Brazilian Institute of Geography and Statistics (IBGE-PPP). IBGE-PPP is a free online service for GNSS (Global Navigation Satellite System) data post-processing that makes use of the GPS Precise Point Positioning (CSRS) program developed by the Geodetic Survey Division of Natural Resources of Canada. It allows users with GPS and/or GLONASS receivers to obtain coordinates referenced to SIRGAS2000 (Geocentric Reference System for the Americas) and ITRF (International Terrestrial Reference Frame) through precise processing.

185 Finally, the reduction level (RL) orthometric altitude was obtained by mathematical subtraction operations at the RN-2 (DHN) level reference orthometric altitude, Eq. (4):

$$H(RL) = H(RN) - 4.046m = 2.92m - 4.046m = -1.126m, \quad (4)$$

### 3.3 LiDAR Digital Elevation Model

An airborne LiDAR DEM was used, with 1m horizontal spatial resolution and coverage for the entire local area. This DEM  
190 was built by PETROBRAS, granted in terms of technical cooperation between the said institution and the Federal University  
of Rio Grande do Norte (UFRN) and made available by the Graduate Program in Geodynamics and Geophysics (PPGG),  
utilizing a confidentiality agreement. The survey took place between February and September 2012, through integrated aero  
photogrammetry. In this aerial survey, a model ALS60 equipment manufactured by Leica Geosystems was used. The average  
point density was 4.2 per m<sup>2</sup>, with a frequency of 200,000 pulses per second (200 kHz) and a 26 ° aperture angle (FOV). The  
195 operating frequency adopted was 160.2 kHz, with 65 Hz profiling frequency and an average aircraft speed of 190 km / h. The  
average point spacing was 0.41 m (in the flight direction) and 0.80 m in the transverse flight direction. The geodetic reference  
system adopted for planimetry was SIRGAS2000. For altimetry, the geoidal model MAPGEO2015 was used. The geometric  
altitude was converted to orthometric altitude to leave all in the same altimetric reference (All linked to the Brazilian Geodetic  
System). The altimetric RMSE of this product, obtained during the evaluation and calibration process (Araújo et al., 2018),  
200 was 0.1704 m.

### 3.4 Scenarios for mean sea level rise (MSL)

Sea level rise has been widespread in the international community as one of the impacts related to climate change, where most  
estimates are projected by the year 2100. For this work we adopted 3 scenarios of sea level rise at a global and regional level,  
to incorporate the predictions of average sea level rise until the year 2100. Was used the forecast scenarios of the  
205 Intergovernmental Panel on Climate Change (IPCC) (RCP 4.5 = 0.53m and RCP 8.5 = 0.74m) (Church et al., 2013) and of  
Brazilian Institute of Geography and Statistics (IBGE) ( $\Delta$ MLS = 2.1mm/year) (IBGE, 2016). RCPs are scenarios with a global  
projection, whereas the IBGE scenario is a projection at a regional level (for Brazilian northeaster. The latter, result of reports  
on data from IBGE tidal network. In all rate of sea level rise in scenarios used, are from robust modelling of sea level projection  
under face climate change.

210

### 3.5 Land use and cover map

Land use and cover mapping of study area was carried out in three stages arranged in a systematic way: 1) Digital Image  
Processing (DIP); 2) fieldwork; 3) cartographic digitization.

The first stage consisted of highlighting thematic information using DIP techniques on multispectral optical images from  
215 LANDSAT-8 platform OLI sensor, and Synthetic Aperture Radar (SAR) multilook Fine image from RADARSAT-2 mission.  
The DIO techniques included band ratios and Principal Components (PCs) applied in the RGB system and RGBIntensity  
hybrid system. Thus, the colored compositions R(7/5)G(6/4)B(5/4), R(PC5)G(PC6)B(PC7) and hybrid composition  
R(7/5)G(6/4)B(5/4)I(RADARSAT-2) were elaborated in order to highlight thematic classes associated with the compositional

differences of the soil, vegetation, water and anthropic materials. PCs 5, 6 and 7 showed a predominant contribution of 58% of band 6, 56% of band 4 and 60% of band 1, respectively, elucidating information from the middle, near and visible infrared spectrum. The use of RADARSAT-2 image sought to extract the maximum textural information from each target on the surface, due to the principles of diffuse and specular reflection of SAR images (Jensen, 2009).

The second stage consisted of an in loco visit of study area in order to validate information extracted from DIP, in addition to providing analyzes on a detailed scale. Correlations were made between observations in field and the land use and cover classes, recognized through spectral data.

Finally, in third stage, all the information on the land use and cover mapping was integrated and mapped by manual vectorization on a scale of 1:10,000 with ArcMap 10 software.

### 3.6 Tidal Flood Risk Mapping

For this work we adopted as a quantitative risk, the likelihood of harmful consequences or expected losses (dead, injured, destroyed and damaged buildings, etc.) occurring as a result of interactions between a natural hazard and conditions of local vulnerability (UNDP, 2004). The formula proposed by Wisner et al. (2011), where the same concept was one of the references of the fifth IPCC report (IPCC, 2014), Eq. (5):

$$\text{Risk map} = \text{Hazard map} \times \text{Vulnerability map}, \quad (5)$$

Where, Hazard map is the likelihood of the process occurring with magnitude  $M$  (destructive potential) and Vulnerability map (physical vulnerability) is the degree of damage or loss to the exposed environment as a result of the impact and as a function of magnitude  $M$ .

For hazard mapping flooding was assigned 4 classes based on the scenarios understudy, in addition to the current flooding (Table 1). Each class represented the quota resulting from the sum of:

- + Projection of MSL elevation to 2100;
- + Meteorological tide (Tr20);
- + Astronomical tide linked to SGB (Tr20);
- + RMSE of DEM.

For the construction of the flood vulnerability mapping, was used as basis the land use land cover mapping previously elaborate this job.. The land use and cover mapping vector file were transformed into a raster file, with a spatial resolution of 1m, due to the spatial resolution of the altimetric data (DEM data). Finally, the raster file was reclassified with vulnerability values, in scores from 0 (no vulnerable) to 5 (most vulnerable), assigned to land use and cover category (Table 2).

After obtaining the flood hazard and vulnerability maps, the risk map was obtained using the risk equation mentioned above. The risk was classified into 5 cassettes, according to the values in Table 3.



## 4 Results and discussion

250 The flood risk mapping from high-resolution DEM provides the knowledge to optimize investments and provide flood risk management in high accuracy (Schröter et al., 2018). The standardized altimetric reference at centimeter intervals become essential, especially when there is an interest in the analysis of land use and cover, or when economic activities occur in these environments, in order to estimate risks with accuracy (Aguar et al., 2019).

The flood quota reached on a region is a particularly complex phenomenon, both in the number of elements involved in the flooding process and in the interaction between these elements. However, it was possible to robustly model the complexity of tidal flooding that occurred in the Piranhas-Açu Estuary, as well as the risk in its probabilistic potential for the coming years.

### 4.1 Tidal behavior and return period

The effect of AT and MT on the coast is observed as a variation of sea level or free surface and it is at this level that waves propagate (SMC-Brasil, 2018). From the GOS data and DHN data applied in this work, it was possible to observe the tidal behaviour in the tropical Piancó-Piranhas-Açu estuary (Figure 4).

The meteorological surge or storm surge is a sea level fluctuation caused by weather effects mainly derived from wind and variations in pressure fields. Throughout the 61 years of data from the GOS point, the maximum annual quota of the meteorological tide presented an average of 12cm and an amplitude of 14cm, with a maximum of 22cm and a minimum of 8cm, in the years 1964 and 1958, respectively. When applying the Mann-Kendall test, no statistically significant trend ( $\tau = -0.123$ ;  $p = 0.16147$ ) was observed in the dataset.

The astronomical tide is the result of the interaction of the gravitational forces of Earth, Moon and the Sun, being completely predictable. With the DHN data set provided by the Brazilian Navy, it was observed that the maximum annual astronomical tide quota presented an average of 2.80 m and a 13 cm amplitude, with a maximum of 2.84 m and a minimum of 2.71 m. In the same study, when the Mann-Kendall test was applied, no statistically significant trend was observed ( $\tau = 0$ ;  $p = 1$ ), showing a steady pattern.

The descriptive values on the tides presented to corroborate the values found in the literature. Frota et al. (2016), studying the tidal behaviour in the Brazilian Northeast during the period from 2009 to 2011 in buoys about 200 km from the Piranhas-Açu estuary, found that the average maximum tide height was 2.79 m, ranging from 2.23 at 3.34 m. In the same study, Frota et al. (2016) found that the sea level variability in the sub-FT (The non-astronomical sea level signal) represents low oscillation, with a maximum of 0.12 m. Mattos et al. (2019), conducted a campaign from December 2010 to February 2011 to study significant wave heights, found that the tide table of Guamaré-RN (approximately 40km East of the table of Macau-RN) had averages of 2.34 m (in syzygy tides) and 2.21 m (in quadrature tides), both above the reduction level.

Regarding the return period ( $T_{r20years}$ ), estimated by the Gumbel distribution function, the values of 15.90 cm and 2.90 m were found for MT and AT, respectively (Figure 5).

280 By performing the geodetic tracking of the DHN RN-2 framework, the ruler was adjusted to the Brazilian Geodetic System (SGB) and in this, the Reduction Level (RL) orthometric altitude, represented by the value of -1.126 m (Figure 3). Thus, the orthometric altitude of the maximum astronomical tide quota for the 20-year return period was 1.777 m, which served as a start for flood models.

#### 4.2 Tidal flood hazard and vulnerability maps

285 It was possible to produce the four classes tidal flood hazard map for the study area based on the mean sea level projection values for the year 2100 (Table 5.4). In this product, the use of the astronomical tide quota linked to the Brazilian Geodetic System (SGB) was of paramount importance, thus ensuring that all input variables for flood hazard mapping were in the same geodetic framework.

After the spatialization of the classes in a GIS environment, the spatial behaviour of the tidal flood hazard throughout the Piranhas-Açú estuary was verified (Figure 6a). In general, there was a positive north-south gradient, with a predominance of the flood class of the present scenario (high hazard). The high hazard class represented 257.60 km<sup>2</sup> of the estuary flood hazard, while the moderate hazard, low hazard, and extremely low hazard classes represented 286.26, 338.67 and 359.42 km<sup>2</sup>, respectively.

Tidal flood stains were observed inside the urban area of the city of Macau. These spots are justified by the current layout of the city's drainage system, where at high tide times seawater enters the galleries and canals, affecting the interior of the city (Figure 6b and Figure 7). Aguiar et al. (2019) found the same structural problem in the urban area of Areia Branca city (approximately 58 km west of Macau city). It is important to mention that the land on which the local cemetery is in the urban area of Macau is one of the few urban sectors in the city not to suffer from tidal flood scenarios.

It was found that the flood event of January 3, 2015, had an orthometric altitude of 1.73m (Figure 8). The same spatial pattern of tidal flooding was observed between the photographic record and the flood model proposed in this work. Thus, validating the applied flood model.

By mapping the land use and land cover, it was obtained the quantification of the areas of the mapped units (Table 5 and Figure 9), highlighting the Caatinga area, which corresponded to 657.18 km<sup>2</sup>.

Regarding the vulnerability map, it was observed that 66.86% (883.84km<sup>2</sup>) of the vulnerable areas had low flood vulnerability (Table 5.5 and Figure 10). However, it is important to note that 16% of vulnerable areas have High and Extremely High vulnerability, corresponding to an area of 205.30 km<sup>2</sup>.

#### 4.3 Tidal flood risk map

From the result of flood hazard and vulnerability mappings, the flood risk map was obtained (Figure 11).

The risk areas represent a total of approximately 360km<sup>2</sup>, where the 135.23km<sup>2</sup> low-risk class stands out. While the other classes represented 85.64km<sup>2</sup> (extremely low risk), 20.25km<sup>2</sup> (moderate risk), 117.73km<sup>2</sup> (high risk) and 0.53km<sup>2</sup> (extremely

high-risk). Extremely high-risk environments were sections of the urban areas of the cities of Porto do Mangue and Macau, and the communities of Ponta do Mel, Rosado and Diogo Lopes (Figure 10).

## 5 Conclusions

The rising of the sea level by a few millimeters per year is an important variable, as loss of land in lowland areas can quickly  
315 destroy coastal ecosystems such as lagoons, lagunas, and mangroves. In addition to flooding of socio-economically and  
environmentally sensitive and relevant areas, the rising sea levels can change the energy balance of coastal environments,  
causing large variations in the sedimentary process and consequently erosion of large stretches of the shoreline. (Castro et al.,  
2010). In the Piranhas-Açu Estuary, sea level rise was not statistically significant, we believe that the temporal scale of our  
meteorological tide data set (1948 to 2008) favoured the masking of this phenomenon. Whereas, it has been noticeable by the  
320 local community and the news for the last 10 years only.

Possibly, tidal flooding in the region under study is closely linked to rising sea levels in recent years. Extreme tidal weather  
events are the main factor in flood danger. Flood hazard, vulnerability and risk maps are crucial for planning and intervention  
in flood prone areas. The case study results in the Piranhas-Açu Estuary can be used by local environmental management,  
mainly to characterize risk zones and to support the implementation of tidal flood risk management plans in this coastal area.  
325 The methodology and materials applied to this study area have proven to be effective in identifying tidal flood risk areas using  
high-resolution DEM that has been calibrated based on high precision GNSS, historical tidal quota data and geoprocessing  
techniques.

It is noteworthy that the methodological approach to the Piranhas-Açu Estuary is suitable to be replicated to other estuaries,  
particularly those in the Brazilian semiarid regions (estuaries with low hydrological contribution from rivers). Tidal flood risk  
330 mapping methodology may be particularly useful for regions with a good historical series of tide data. In this case study, the  
tide flood event modelling of 2015 was compared with the photographic records of the respective event and established high  
visual similarity between them.

This paper also demonstrates that well-applied geoprocessing techniques such as GIS and high precision geodesic provide  
results that can be very effective in environmental management with low-cost investments, highlighting the unique features of  
335 a given locality, especially floodplains and wetlands.

## Conflicts of interest

None.

## Acknowledgments

The authors express special thanks to the PETROBRAS for providing Digital Elevation Model LiDAR data. We also thank  
340 the reviewers of the Natural Hazards and Earth System Sciences (NHES) journal for their many insightful comments.

## References

- Aguiar, L. S., Amaro, V. E., Araújo, P. V. N., and Santos, A. L. S.: Geotecnologias de Baixo Custo Aplicadas à Avaliação de Risco por Inundação em Áreas Urbanas Costeiras em Cenários de Mudanças Climáticas, *Anuário do Instituto de Geociências – UFRJ*, 42, 267-290, [http://dx.doi.org/10.11137/2019\\_1\\_267\\_290](http://dx.doi.org/10.11137/2019_1_267_290), 2019.
- 345 Amaro, V. E.; Santos, M. S. T.; Souto, M. V. S.: Geotecnologias Aplicadas ao Monitoramento Costeiro: Sensoriamento Remoto e Geodésia de Precisão. 1ª Ed, Edição dos Autores, Natal, RN, 118 pp., 2012.
- ANA - Agência Nacional das Águas: Plano de recursos hídricos da bacia hidrográfica do rio Piancó-Piranhas-Açu, Brasília-DF, 167 pp., available at: [http://piranhasacu.ana.gov.br/produtos/PRH\\_PiancoPiranhasAcu\\_ResumoExecutivo\\_30062016.pdf](http://piranhasacu.ana.gov.br/produtos/PRH_PiancoPiranhasAcu_ResumoExecutivo_30062016.pdf) (last access: 25 June 2019), 2016.
- 350 Araújo, P. V. N., Amaro, V. E.; Alcoforado, A. V. C., and Santos, A. L. S.: Acurácia Vertical e Calibração de Modelos Digitais de Elevação (MDEs) para a Bacia Hidrográfica Piranhas-Açu, Rio Grande do Norte, Brasil, *Anuário do Instituto de Geociências – UFRJ*, 41, 351–364, [https://doi.org/10.11137/2018\\_1\\_351\\_364](https://doi.org/10.11137/2018_1_351_364), 2018.
- Araújo, P. V. N, Amaro, V. E., Silva, M. S. and Lopes, A. B.: Delimitation of flood areas based on a calibrated a DEM and geoprocessing: case study on the Uruguay River, Itaqui, southern Brazil, *Natural Hazards and Earth System Sciences*, 19, 237-  
355 250, <https://doi.org/10.5194/nhess-19-237-2019>, 2019.
- Bamber, J. L., Oppenheimer, M., Kopp, R. E., Aspinall, W. P. and Cooke, R. M.: Ice sheet contributions to future sea-level rise from structured expert judgment, *Proceedings of the National Academy of Sciences*, 116, 11195-11200, <https://doi.org/10.1073/pnas.1817205116>, 2019.
- Barbosa, M. E. F., Boski, T., Bezerra, F. H. R., Gomes, M. P., Lima-Filho, F. P., Pereira, L. C., and Maia, R. P.: Late Quaternary  
360 infilling of the Assu River embayment and related sea level changes in NE Brazil, *Marine Geology*, 405, 23-37, <https://doi.org/10.1016/j.margeo.2018.07.014>, 2018a.
- Barbosa, M. E. F., Bezerra, F. H. R., Boski, T., Lima-Filho, F. P., and Valdevino, D. S.: Padrões geomorfológicos na região estuarina do Rio Assu, NE – Brasil, *Revista Brasileira de Geomorfologia*, 19, 525-545, <http://dx.doi.org/10.20502/rbg.v19i3.1208>, 2018b.
- 365 Boori, M. S., Amaro, V. E. and Targino, A.: Coastal risk assessment and adaptation of the impact of sea-level rise, climate change and hazards: A RS and GIS based approach in Apodi-Mossoró estuary, Northeast Brazil, *International Journal of Geomatics and Geosciences*, 2, 815-832, 2012.
- Brasil: Plano Nacional de Adaptação à Mudança do Clima, estratégias setoriais e temáticas, Ministério do Meio Ambiente, Brasília-DF, v.2, 295 pp., available at:

- 370 [https://www.mma.gov.br/images/arquivo/80182/LIVRO\\_PNA\\_Plano%20Nacional\\_V2\\_copy\\_copy.pdf](https://www.mma.gov.br/images/arquivo/80182/LIVRO_PNA_Plano%20Nacional_V2_copy_copy.pdf) (last access: 12 April 2019), 2016.
- Busman, D. V., Amaro, V. E. and Souza-Filho, P. W. M.: Análise Estatística Multivariada de Métodos de Vulnerabilidade Física em Zonas Costeiras Tropicais. *Revista Brasileira de Geomorfologia*, 17, 499-516, <http://dx.doi.org/10.20502/rbg.v17i3.912>, 2016.
- 375 Castro, B. M., Brandini, F. P., Wainer, I. E. K. C. and Dottori, M.: O mar de amanhã, com as mudanças climáticas de hoje, *Ciência e Cultura*, 62, 40-42, available at: <http://cienciaecultura.bvs.br/pdf/cic/v62n3/a16v62n3.pdf> (last access: 11 November 2019), 2010.
- CHM – Centro de Hidrografia da Marinha. Marinha do Brasil: Sondagem batimétrica, available at: <https://www.marinha.mil.br/chm/dados-do-segnav-lev-hidro/sondagem-batimetrica> (last access: 20 April 2019), 2019a.
- 380 CHM – Centro de Hidrografia da Marinha. Marinha do Brasil. Maregrafia e fluviometria. available at: <https://www.marinha.mil.br/chm/dados-do-segnav-lev-hidro/maregrafia-e-fluviometria> (last access: 20 April 2019), 2019b.
- Costa, L. R. F., Maia, R. P., Barreto, L. L., and Sales, V. C. C.: Geomorfologia do nordeste setentrional brasileiro: uma proposta de classificação, *Revista Brasileira de Geomorfologia*, 21, 185-208, <http://dx.doi.org/10.20502/rbg.v21i1.1447>, 2020.
- Dahl, K. A., Fitzpatrick, M. F., and Spanger-Siegfried, E.: Sea level rise drives increased tidal flooding frequency at tide gauges along the U.S. East and Gulf Coasts: Projections for 2030 and 2045, *PLoS ONE*, 12, e0170949, <http://dx.doi.org/10.1371/journal.pone.0170949>, 2017.
- 385 Church, J. A., Clark, P. U., Cazenave, A., Gregory, J. M., Jevrejeva, S., Levermann, A., ... Unnikrishnan, A. S.: Sea level change. In T. F. Stocker, D. Qin, G.-K. Plattner, M. Tignor, S. K. Allen, J. Boschung, et al. (Eds.), *Climate Change 2013: The Physical Science Basis. Contribution of Working Group 1 to the Fifth Assessment Report of the Intergovernmental Panel on Climate Change* (pp. 1137– 1216). Cambridge, England and New York, NY: Cambridge University Press, 2013.
- 390 Dangendorf, S., Hay, C., Calafat, F. M., Marcos, M., Piecuch, C. G., Berk, K. and Jensen, J.: Persistent acceleration in global sea-level rise since the 1960s, *Nature Climate Change*, 9, 705-710, <https://doi.org/10.1038/s41558-019-0531-8>, 2019.
- DHN - Diretoria de Hidrografia e Navegação: Tábuas de marés, available at: <https://www.marinha.mil.br/chm/tabuas-de-mare> (last access: 3 January 2018), 2018.
- 395 Diniz, C. H. G., Amaro, V. E., Prudêncio, M. C. and Felipe R. F.: Representação Tridimensional de Processos de Erosão Costeira em Ilhas Barreiras Utilizando Tecnologia de Jogos, *Anuário do Instituto de Geociências – UFRJ*, 40, 147-158, [http://dx.doi.org/10.11137/2017\\_3\\_147\\_158](http://dx.doi.org/10.11137/2017_3_147_158), 2017.
- Diniz, M. T. M. and Pereira, V. H. C.: Climatologia do Estado do Rio Grande do Norte, Brasil: sistemas atmosféricos atuantes e mapeamento de tipos de clima, *Boletim Goiano de Geografia*, 35, 488-506, <https://doi.org/10.5216/bgg.v35i3.38839>, 2015.
- 400 Dwarakisha, G. S., Vinaya, S. A., Natesanb, U., Asanoc, T., Kakinumac, T., Venkataramanad, K., Paia, B. J. and Babitaa, M. K.: Coastal vulnerability assessment of the future sea level rise in Udupi coastal zone of Karnataka state, west coast of India, *Ocean & Coastal Management*, 52, 467-478, <https://doi.org/10.1016/j.ocecoaman.2009.07.007>, 2009.

- Easterling, D. R., Meehl, G. A., Parmesan, C., Changnon, S. A., Karl, T. R. and Mearns, L. O.: Climate Extremes: Observations, Modeling, and Impacts, *Science*, 289, 2068–2074, <http://dx.doi.org/10.1126/science.289.5487.2068>, 2000.
- 405 Frota, F. F., Truccolo, E. C. and Schettini, C. A. F.: Tidal and sub-tidal sea level variability at the northern shelf of the Brazilian Northeast Region, *Anais da Academia Brasileira de Ciências*, 88, 1371-1386, <http://dx.doi.org/10.1590/0001-3765201620150162>, 2016.
- Gilleland, E. and Katz, R. W.: extRemes 2.0: An Extreme Value Analysis Package in R, *Journal of Statistical Software*, 72, 1-39, <http://dx.doi.org/10.18637/jss.v072.i08>, 2016.
- 410 Grigio, A. M., Castro, A. F., Souto, M. V. S., Amaro, V. E., Vital, H. and Diodato, M. A.: Use of remoting sensing and geographical information system in the determination of the natural and environmental vulnerability of the Municipal District of Guamaré - Rio Grande do Norte - Northeast of Brazil, *Journal of Coastal Research, Special Issue*, 1427-1431, [www.jstor.org/stable/25742990](http://www.jstor.org/stable/25742990) (last access: 22 December 2019), 2006.
- Gumbel, E. J.: *Statistics of extremes*. Columbia University Press, New York, 375 pp., 1958.
- 415 Hall, J. W., Harvey, H. and Manning, L. J. Adaptation thresholds and pathways for tidal flood risk management in London, *Climate Risk Management*, 24, 42–58, <https://doi.org/10.1016/j.crm.2019.04.001>, 2019.
- Herdman, L., Erikson, L. and Barnard, P.: Storm Surge Propagation and Flooding in Small Tidal Rivers during Events of Mixed Coastal and Fluvial Influence, *Journal of Marine Science and Engineering*, 6, 158, <https://doi.org/10.3390/jmse6040158>, 2018.
- 420 IBGE - Instituto Brasileiro de Geografia e Estatística: Análise do Nível Médio do Mar nas Estações da Rede Maregráfica Permanente para Geodésia – RMPG 2001/2015, Diretoria de Geociências, Coordenação de Geodésia, Rio de Janeiro, 65 pp., available at: [ftp://geoftp.ibge.gov.br/informacoes\\_sobre\\_posicionamento\\_geodesico/rmpg/relatorio/relatorio\\_RMPG\\_2001\\_2015\\_GRRV.pdf](ftp://geoftp.ibge.gov.br/informacoes_sobre_posicionamento_geodesico/rmpg/relatorio/relatorio_RMPG_2001_2015_GRRV.pdf) (last access: 25 June 2019), 2016.
- 425 IDEMA - Instituto de Desenvolvimento Sustentável e Meio Ambiente: Informações dos municípios de Mossoró, Grossos e Tibau, v. 24, 1-24, 1999.
- IDEMA - Instituto de Desenvolvimento Sustentável e Meio Ambiente: Projeto de Zoneamento Ecológico-Econômico dos Estuários do Rio Grande do Norte – ZEE/RN, Natal-RN, 35 pp., 2005.
- IPCC: Climate Change 2014: Synthesis Report, Contribution of Working Groups I, II and III to the Fifth Assessment Report  
430 of the Intergovernmental Panel on Climate Change (IPCC), Geneva, Switzerland, 151 pp., 2014.
- Jensen, J. R.: *Sensoriamento Remoto do Ambiente: Uma Perspectiva em Recursos Terrestres*, Tradução da Segunda Edição, Parêntese Editora, São José dos Campos, 598 pp., 2009.
- Kendall, M. G.: *Rank Correlation Methods*, Charles Griffin, London, 1975.
- Kulp, S. and Strauss, B. H.: New elevation data triple estimates of global vulnerability to sea-level rise and coastal flooding,  
435 *Nature Communications*, 10, 4844, <https://doi.org/10.1038/s41467-019-12808-z>, 2019.

- Lima, C. C.: Sensoriamento remoto aplicado à atualização de informações geoambientais e ao estudo da dinâmica da paisagem no estuário do Rio Piranhas-Açu/NE do Brasil, Monographic, Geology degree, Federal University of Rio Grande do Norte, Natal, 141pp., <http://dx.doi.org/10.13140/RG.2.2.26748.08326>, 2016.
- Mann, H. B.: Nonparametric tests against trend, *Econometrica*, 13, 245–259, <https://doi.org/10.2307/1907187>, 1945.
- 440 Matos, M. F. A., Amaro, V. E., Scudelari, A. C. and Bezerra, A. C. N.: Análises estatísticas de alturas significativas de ondas de série temporal de curto prazo na costa do Rio Grande do Norte. *Pesquisas em Geociências*, 46, e0731, <https://doi.org/10.22456/1807-9806.93246>, 2019.
- Matos, A. C. O. C.: Implementação de Modelos Digitais de Terreno para Aplicações na Área de Geodésia e Geofísica na América do Sul, Ph.D. theses, Postgraduate Program in Transport Engineering, Federal University of Sao Paulo, 335 pp.,  
445 <http://dx.doi.org/10.11606/T.3.2005.tde-10102005-104155>, 2005.
- McGranahan, G., Balk, D. and Anderson, B.: The rising tide: assessing the risks of climate change and human settlements in low elevation coastal zones, *Environment and Urbanization*, 19, 17–37, <https://doi.org/10.1177%2F0956247807076960>, 2007.
- Medeiros, M. D.: Eventos hidroclimáticos extremos e vulnerabilidade socioambiental a inundações no Baixo-Açu – RN, Ph.D. theses, Postgraduate Program in Geography, Federal University of Ceara, Brazil, 209 pp., available at:  
450 <http://www.repositorio.ufc.br/handle/riufc/35674> (last access: 22 December 2019), 2018.
- Medeiros, M.D. and Zanella, M.E.: Estudo das vazões e estimativas de inundações no Baixo-Açu-RN, *Geo UERJ*, 40946, 1-30, <http://dx.doi.org/10.12957/geouerj.2019.40946>, 2019.
- Murray, N. J., Phinn, S. R., DeWitt, M., Ferrari, R., Johnston, R., Lyons, M. B., Clinton, N., Thau, D. and Fuller, R. A.: The global distribution and trajectory of tidal flats, *Nature*, 565, 222-225, <https://doi.org/10.1038/s41586-018-0805-8>, 2019.
- 455 Nerem, R. S., Beckley, B. D., Fasullo, J. T., Hamlington, B. D., Masters, D. and Mitchum, G. T.: Climate-change-driven accelerated sea-level rise detected in the altimeter era, *Proc. Natl. Acad. Sci. U.S.A.* 115, 2022–2025, <https://doi.org/10.1073/pnas.1717312115>, 2018.
- Neumann, B., Vafeidis, A. T., Zimmermann, J. And Nicholls, R. J.: Future coastal population growth and exposure to sea-level rise and coastal flooding - a global assessment, *PLOS ONE*, 10, e0131375, <https://doi.org/10.1371/journal.pone.0131375>,  
460 2015.
- Nicholls, R. J. and Cazenave, A.: Sea-level rise and its impact on coastal zones, *Science*, 328, 1517-1520, <http://dx.doi.org/10.1126/science.1185782>, 2010.
- Nicholls, R. J., Wong, P. P., Burkett, V., Codignotto, J., Hay, J., McLean, R., Ragoonaden, S., Woodroffe, C. D., Abuodha, P. A. O., Arblaster, J., Brown, B., Forbes, D., Hall, J., Kovats, S., Lowe, J., McInnes, K., Moser, S., Rupp-Armstrong, S. and  
465 Saito, Y.: Coastal systems and low-lying areas, in: *Climate change 2007: impacts, adaptation and vulnerability. Contribution of Working Group II to the fourth assessment report of the Intergovernmental Panel on Climate Change*, edited by: Parry, M. L., Canziani, O. F., Palutikof, J. P., van der Linden, P. J. and Hanson, C. E., Cambridge, UK, Cambridge University Press, 315-356, available at: <http://ro.uow.edu.au/cgi/viewcontent.cgi?article=1192&context=scipapers> (last access: 22 December 2019), 2007.

- 470 Nicholls, R. J., Hanson, S. E., Lowe, J. A., Warrick, R. A., Lu, X., Long, A. J. and Carter, T. R.: Constructing Sea-Level Scenarios for Impact and Adaptation Assessment of Coastal Areas: A Guidance Document. Technical Guidelines of the Task Group on Data and Scenario Support for Impact and Climate Analysis (TGICA) of the Intergovernmental Panel on Climate Change (IPCC), 64 pp., available at: [https://www.ipcc-data.org/docs/Sea\\_Level\\_Scenario\\_Guidance\\_Oct2011.pdf](https://www.ipcc-data.org/docs/Sea_Level_Scenario_Guidance_Oct2011.pdf) (last access: 5 December 2019), 2011.
- 475 NOAA - National Oceanic and Atmospheric Administration: 2018 State of U.S. High Tide Flooding with a 2019 Outlook, NOAA Technical Report NOS CO-OPS 090, Silver Spring, Maryland, 31p., available at: <https://repository.library.noaa.gov/view/noaa/20691> (last access: 9 November 2019), 2019.
- PBMC - Painel Brasileiro de Mudanças Climáticas: Impactos, vulnerabilidades e adaptação às mudanças climáticas, Contribuição do Grupo de Trabalho 2 do Painel Brasileiro de Mudanças Climáticas ao Primeiro Relatório da Avaliação Nacional sobre Mudanças Climáticas, edited by: Assad, E.D. and Magalhães, A. R., COPPE, Federal University of Rio de Janeiro, Rio de Janeiro, RJ, Brazil, 414 pp., available at: [http://www.pbmc.coppe.ufrj.br/documentos/RAN1\\_completo\\_vol2.pdf](http://www.pbmc.coppe.ufrj.br/documentos/RAN1_completo_vol2.pdf) (last access: 10 October 2019), 2014.
- 480 Pugh, D. T.: Tides, surges and mean sea level: a handbook for Engineers and Scientists, John Wiley & Sons Ltd., New York, available at: <https://eprints.soton.ac.uk/19157/1/sea-level.pdf> (last access: 22 December 2019), 1987.
- 485 R Development Core Team: R: A language and environment for statistical computing, R Foundation for Statistical Computing, Vienna, Austria, available at: <http://www.R-project.org/>, last access: 28 February 2020.
- Ramos, A. M. and Krueger, C. P.: Aplicação de reduções batimétricas GPS em levantamentos hidrográficos, Boletim de Ciências Geodesicas, 15, 615–635, available at: <https://revistas.ufpr.br/bcg/article/view/16284/10775> (last access: 22 December 2019), 2009.
- 490 Schröter, K., Lüdtke, S., Redweik, R., Meier, J., Bochow, M., Ross, L., Nage, C., and Kreibich, H.: Flood loss estimation using 3D city models and remote sensing data, Environmental Modelling and Software, 105, 118-131, <http://dx.doi.org/10.1016/j.envsoft.2018.03.032>, 2018.
- Santos, M. S. T. and Amaro, V. E.: Dinâmica sazonal de processos costeiros e estuarinos em sistema de praias arenosas e ilhas barreira no nordeste do Brasil, Revista Brasileira de Geomorfologia, 14, 151-162, <http://dx.doi.org/10.20502/rbg.v14i2.298>, 2013.
- 495 SMC-Brasil: Níveis e cota de inundação, Documento temático, Ministério do Meio Ambiente, Brasília-DF, 130 pp., [https://www.mma.gov.br/images/arquivo/80342/Livro\\_SMC\\_4\\_\\_\\_Niveis\\_e\\_Cota\\_de\\_inundacao.pdf](https://www.mma.gov.br/images/arquivo/80342/Livro_SMC_4___Niveis_e_Cota_de_inundacao.pdf) (last access: 16 November 2019), 2018.
- Taherkhani, M., Vitousek, S., Barnard P. L., Frazer, N., Anderson, T. R. and Fletcher, C. H.: Sea-level rise exponentially increases coastal flood frequency, Scientific Reports, 10, 6466, <https://doi.org/10.1038/s41598-020-62188-4>, 2020.
- 500 UNDP - United Nations Development Programme: Reducing Disaster Risk: A Challenge for development, A global report, 169 pp., available at: [http://www.planat.ch/fileadmin/PLANAT/planat\\_pdf/alle\\_2012/2001-2005/Pelling\\_\\_Maskrey\\_et\\_al\\_2004\\_-\\_Reducing\\_Disaster\\_Risk.pdf](http://www.planat.ch/fileadmin/PLANAT/planat_pdf/alle_2012/2001-2005/Pelling__Maskrey_et_al_2004_-_Reducing_Disaster_Risk.pdf) (last access 4 December 2019), 2004.



- 505 Wisner, B., Gaillard, J. C. and Kelman, I.: Framing disaster: theories and stories seeking to understand hazards, vulnerability  
and risk, in: *The Routledge Handbook of Hazards and Disaster Risk Reduction*, edited by: Wisner, B., Gaillard, J. C. and  
Kelman I., London, Routledge, 18-33, available at:  
<https://www.routledgehandbooks.com/pdf/doi/10.4324/9780203844236.ch3> (last access: 7 November 2019), 2011.
- Yue, S. and Wang, C.: The Mann–Kendall Test Modified by Effective Sample Size to Detect Trend in Serially Correlated  
Hydrological Series, *Water Resour. Manage.*, 18, 201–218, <https://doi.org/10.1023/B:WARM.0000043140.61082.60>, 2004.
- 510 Zhang, W., Yan, Y., Zheng, J., Li, L., Dong, X., and Cai, H.: Temporal and spatial variability of annual extreme water level  
in the Pearl River Delta region, China, *Global Planet. Change*, 69, 35-47, <https://doi.org/10.1016/j.gloplacha.2009.07.003>,  
2009.

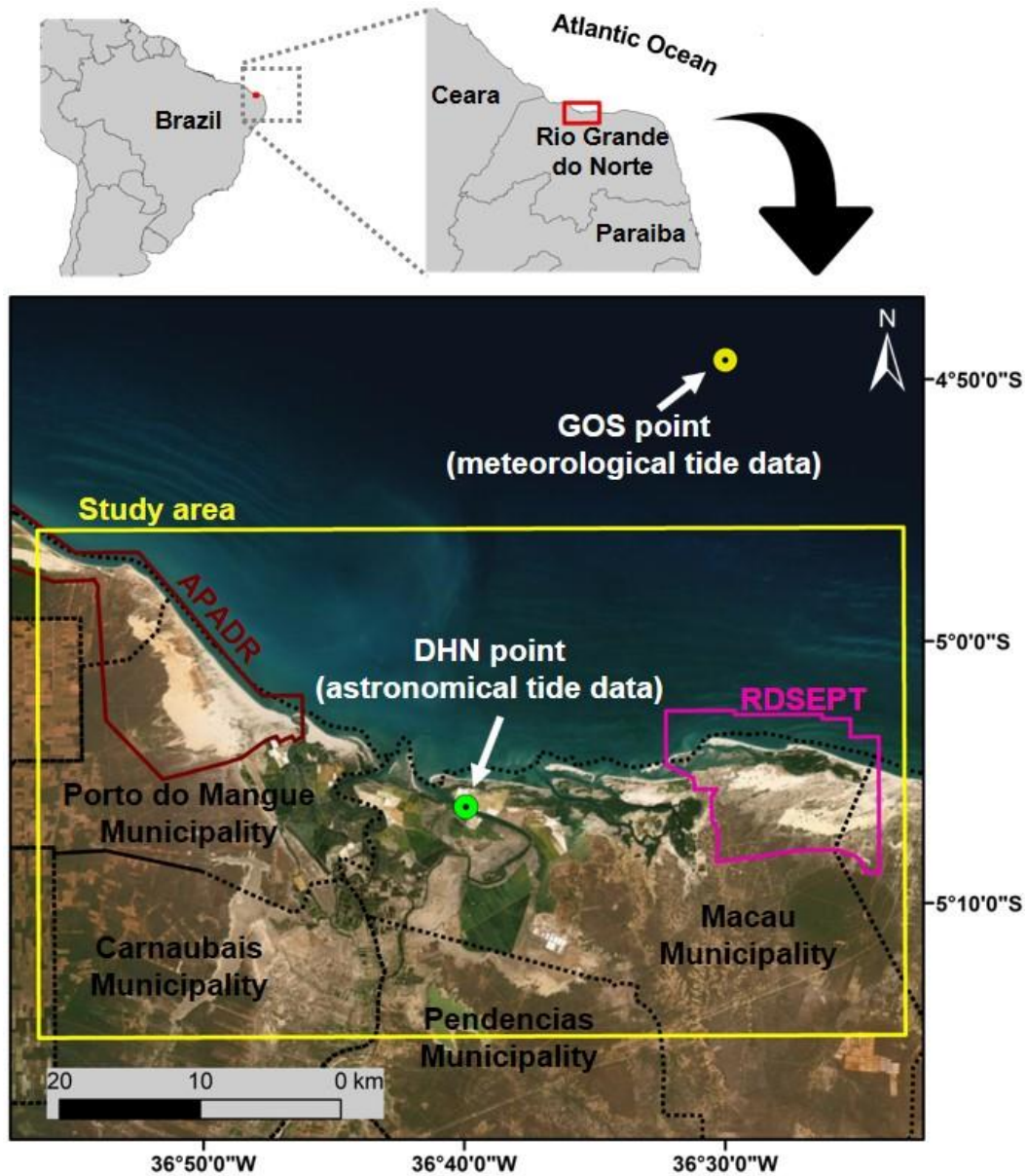
515

520

525

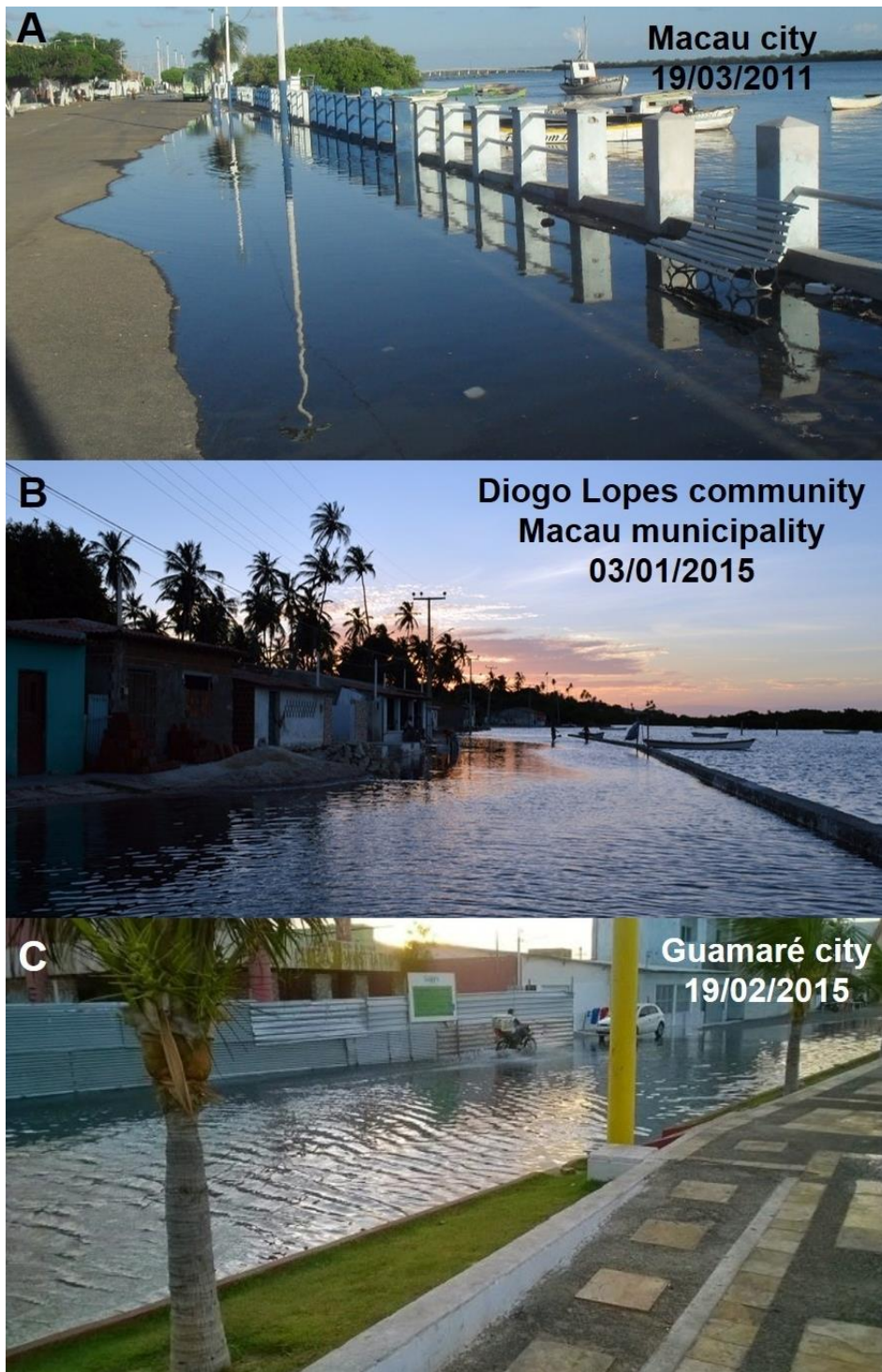
530

535



540

Figure 1: Location of the study area. The yellow rectangle represents the delimitation of the study area: Pianco-Piranhas-Açu estuary and its surroundings. The pink polygon highlights the boundary of the Ponta do Tubarao State Sustainable Development Reserve (RDSEPT), while the burgundy polygon delimits the Rosado Dunes Environmental Preservation Area (APADR). Basemap from ArcGIS Online: © ESRI.



545

**Figure 2: Tidal flooding events in north coastal of Rio Grande do Norte State. (A) Macau urban area, Macau municipality, Mar 19, 2011 (Unknow author); (B) Diogo Lopes community, Macau municipality, Jan 03, 2015 (Tiago Ezequiel); and (C) Guamare urban area, Guamare municipality, Feb 19, 2015 (Unknown author).**

550

555

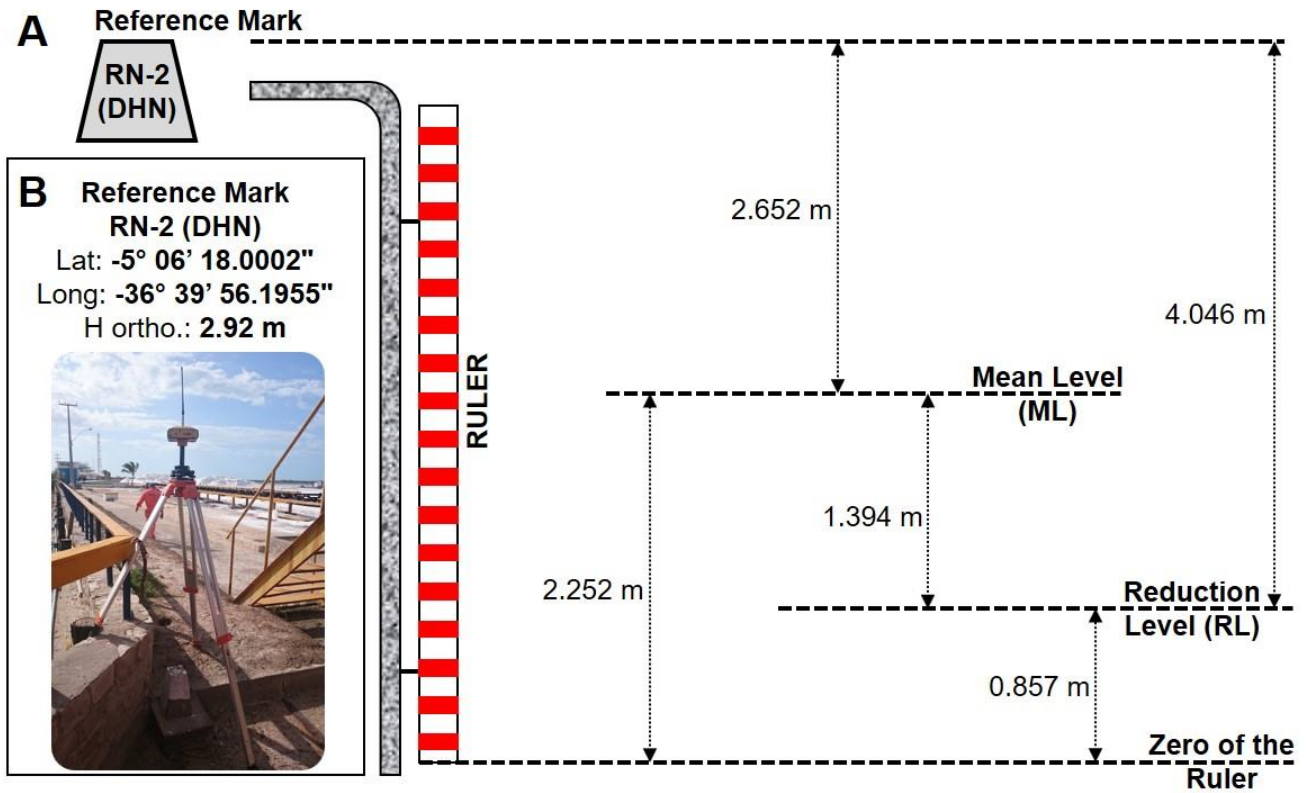
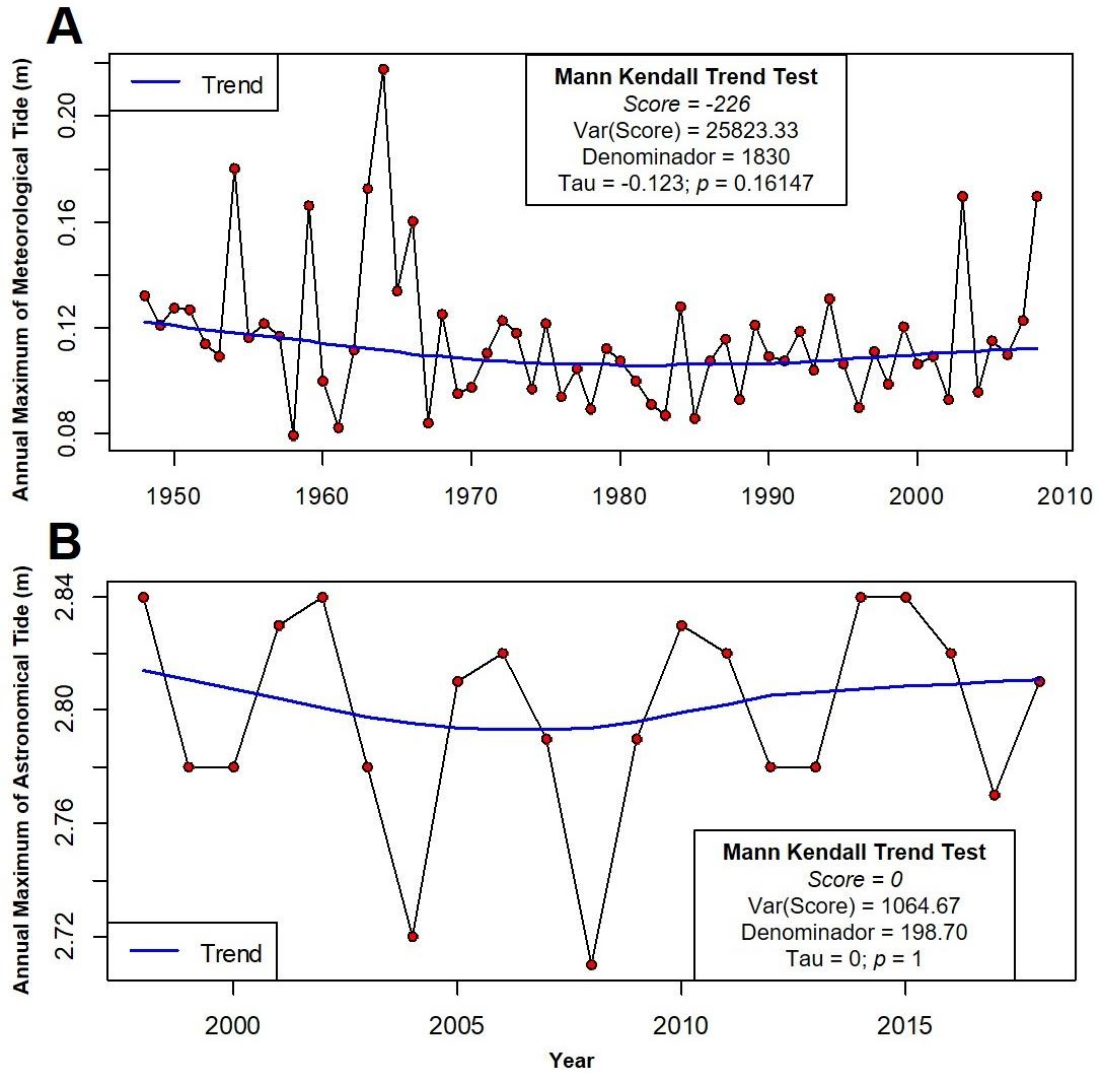


Figure 3: Scheme illustrating the differences in quotas between the references adopted by the Brazilian Navy: (A) Reference Mark RN-2 (DHN); and (B) Coordinates of Reference Mark RN2- (DHN).

560

565



570

Figure 4: Annual tide maximum level temporal serie: (A) Meteorological tide; and (B) Astronomical tide.

575



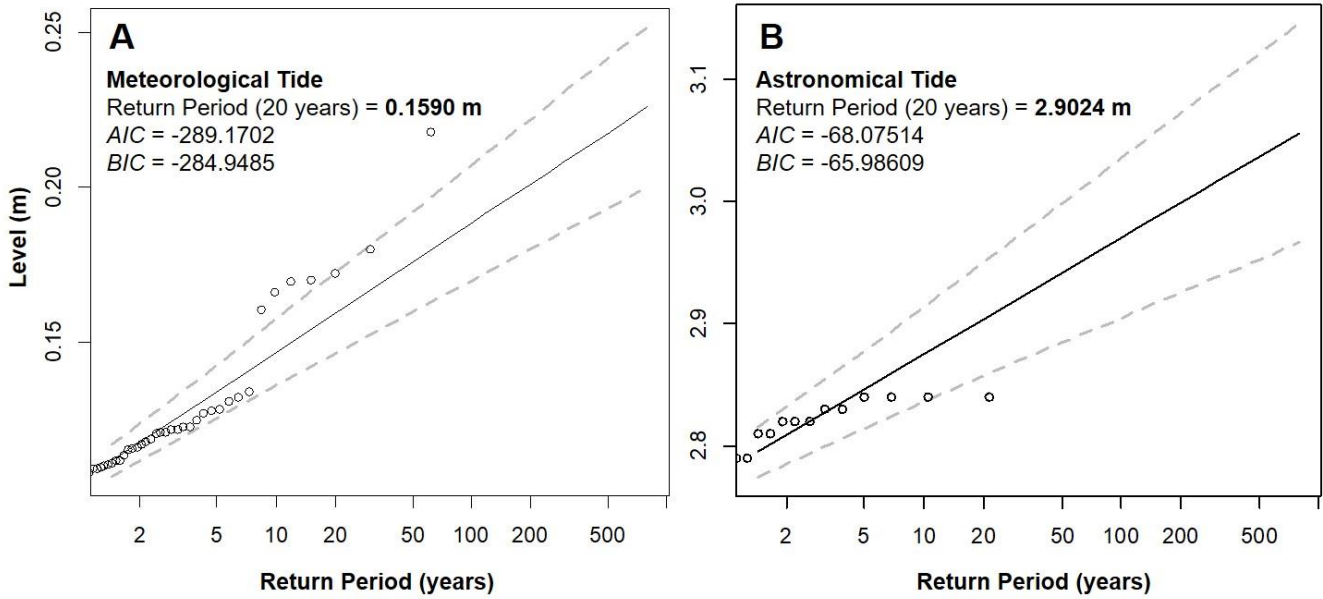


Figure 5: Return period graph of tide data: (A) Meteorological tide; and (B) Astronomical tide.

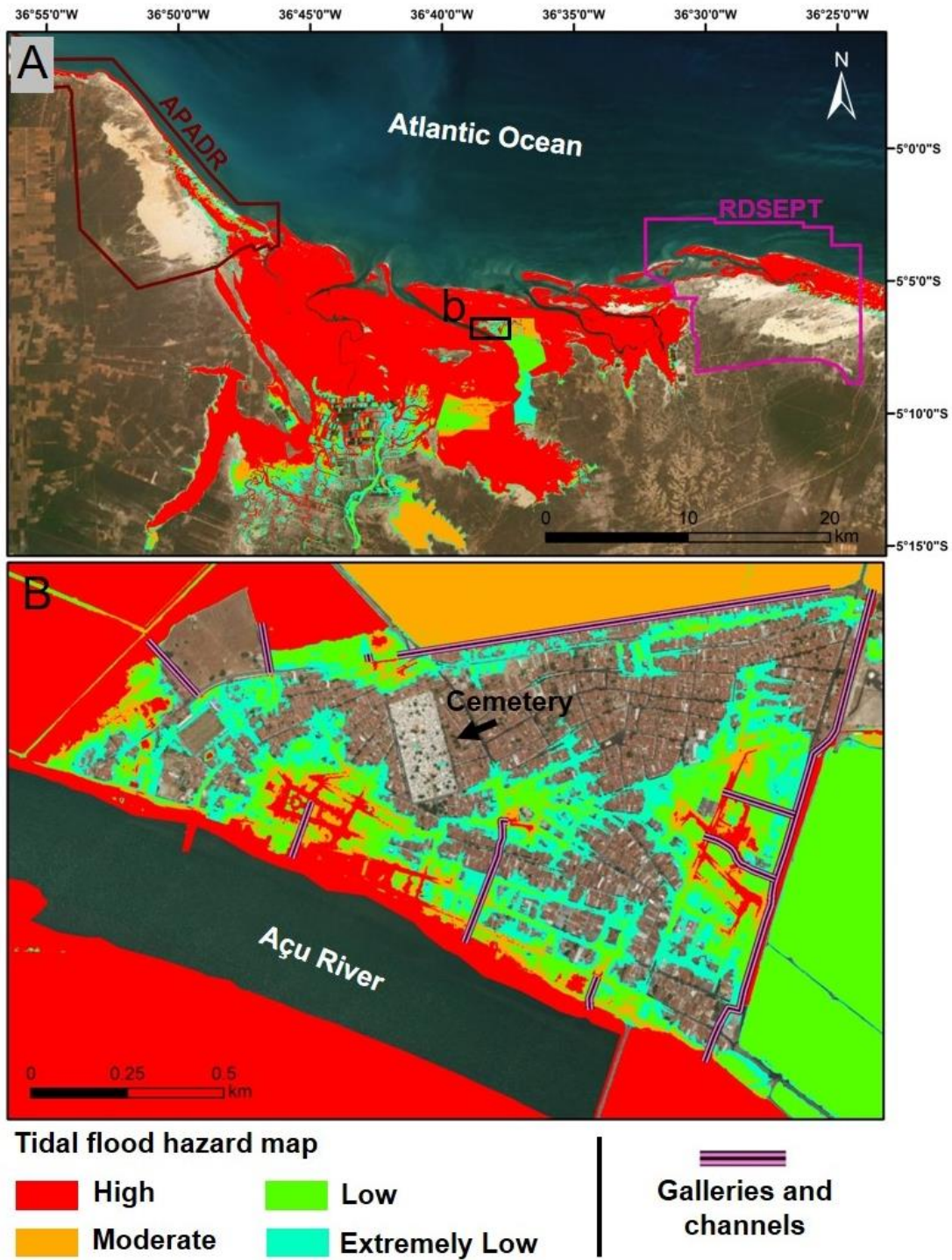
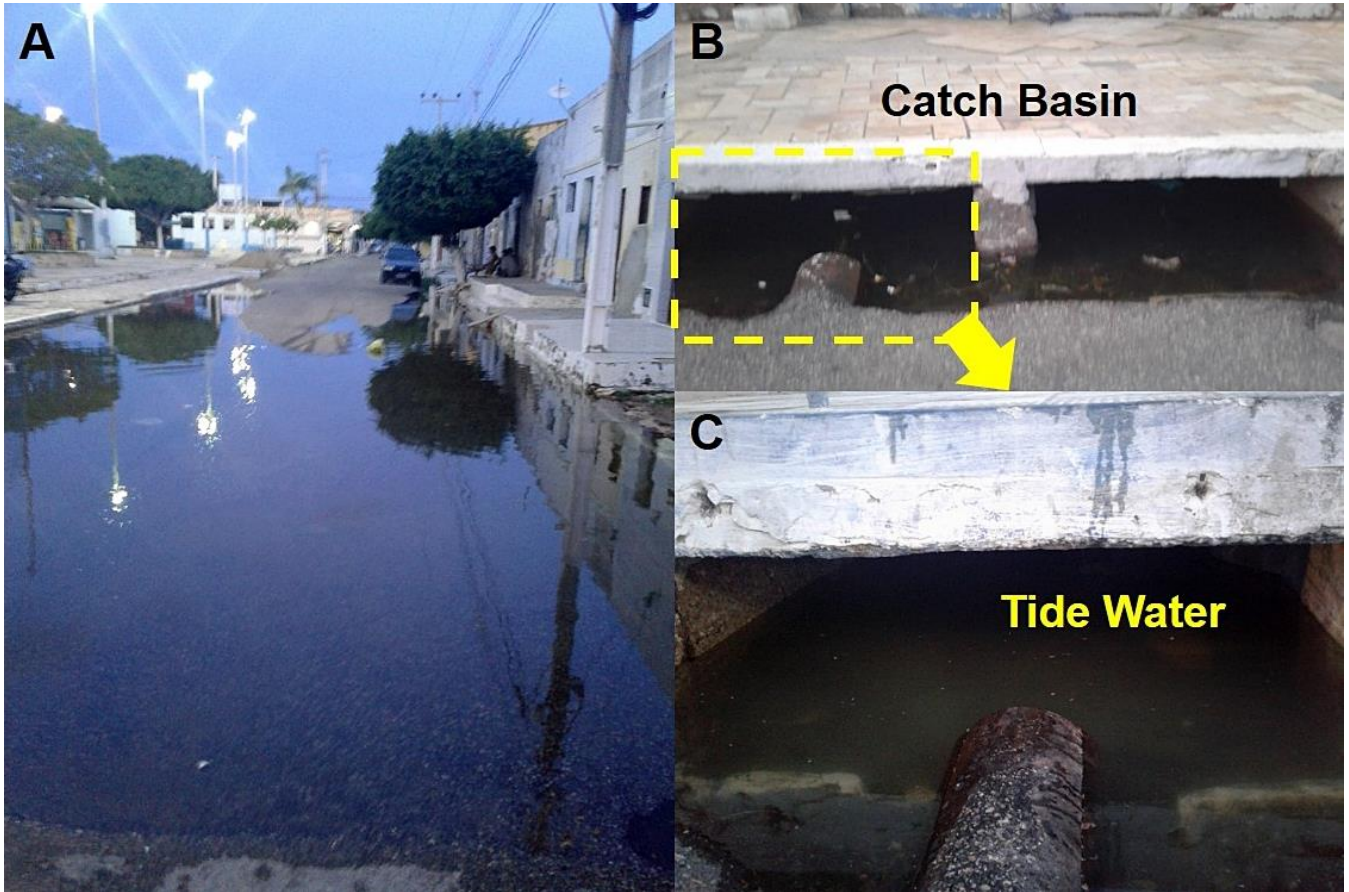
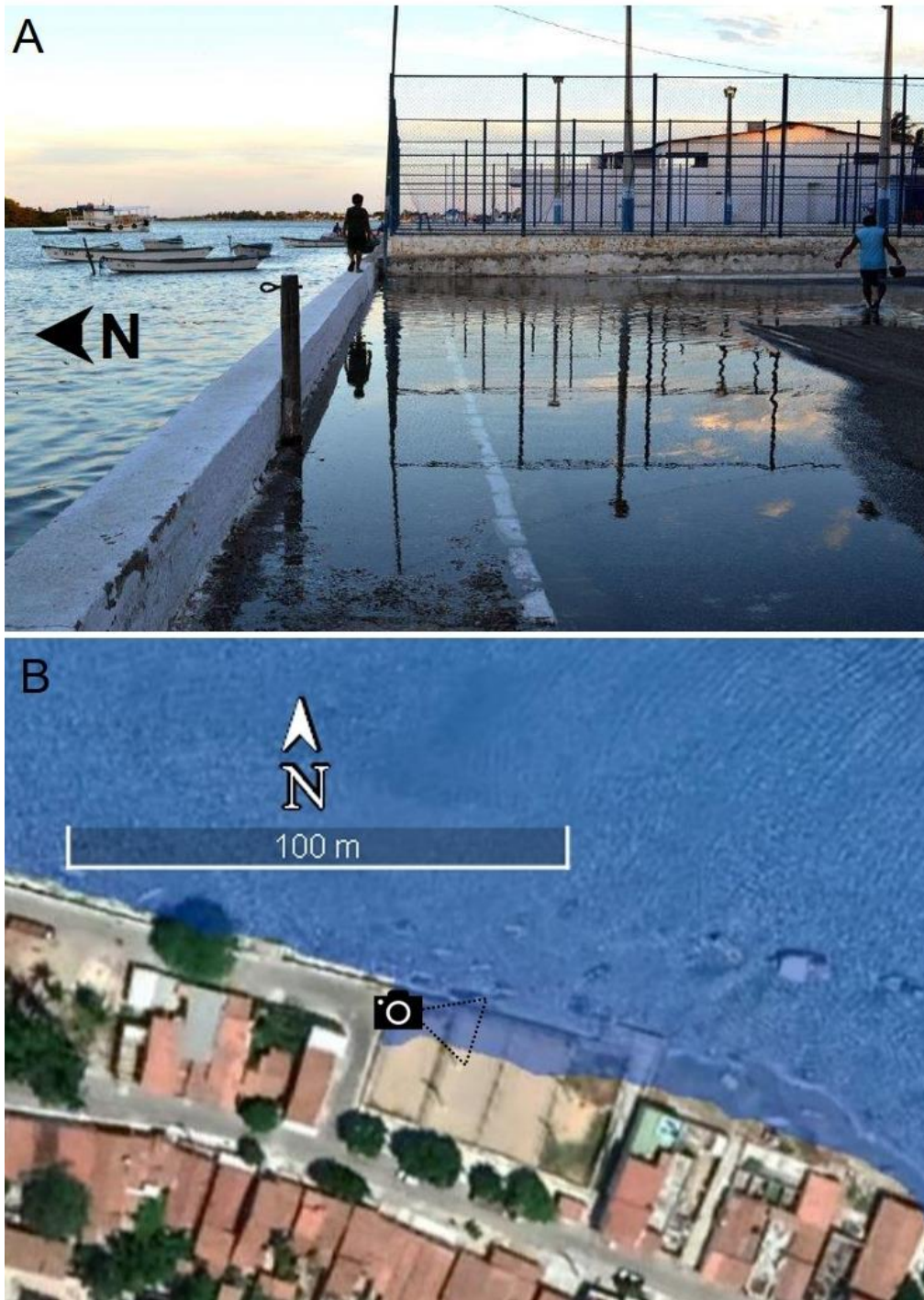


Figure 6: Tidal flood hazard map: (A) Total area under study; and (B) Detail in Macau urban area. Basemap from ArcGIS Online: © ESRI.



595 **Figure 7: Tidal flood through the rain drainage system: (A) Tidal flooding event on March 10, 2020 (Macau urban area); (B) Example of local catch basin; and (C) Catch basin in detail.**





605 **Figure 8: Tidal flooding events in north coastal of Rio Grande do Norte State: (A) Photographic record of Diogo Lopes community, Macau City, on January 3, 2015. (Tiago Ezequiel); and (B) simulated flood event for Diogo Lopes community on January 3, 2015. (orthometric height of tidal flood = 1.73m) (Basemap from Google Earth Pro: © Google LLC).**

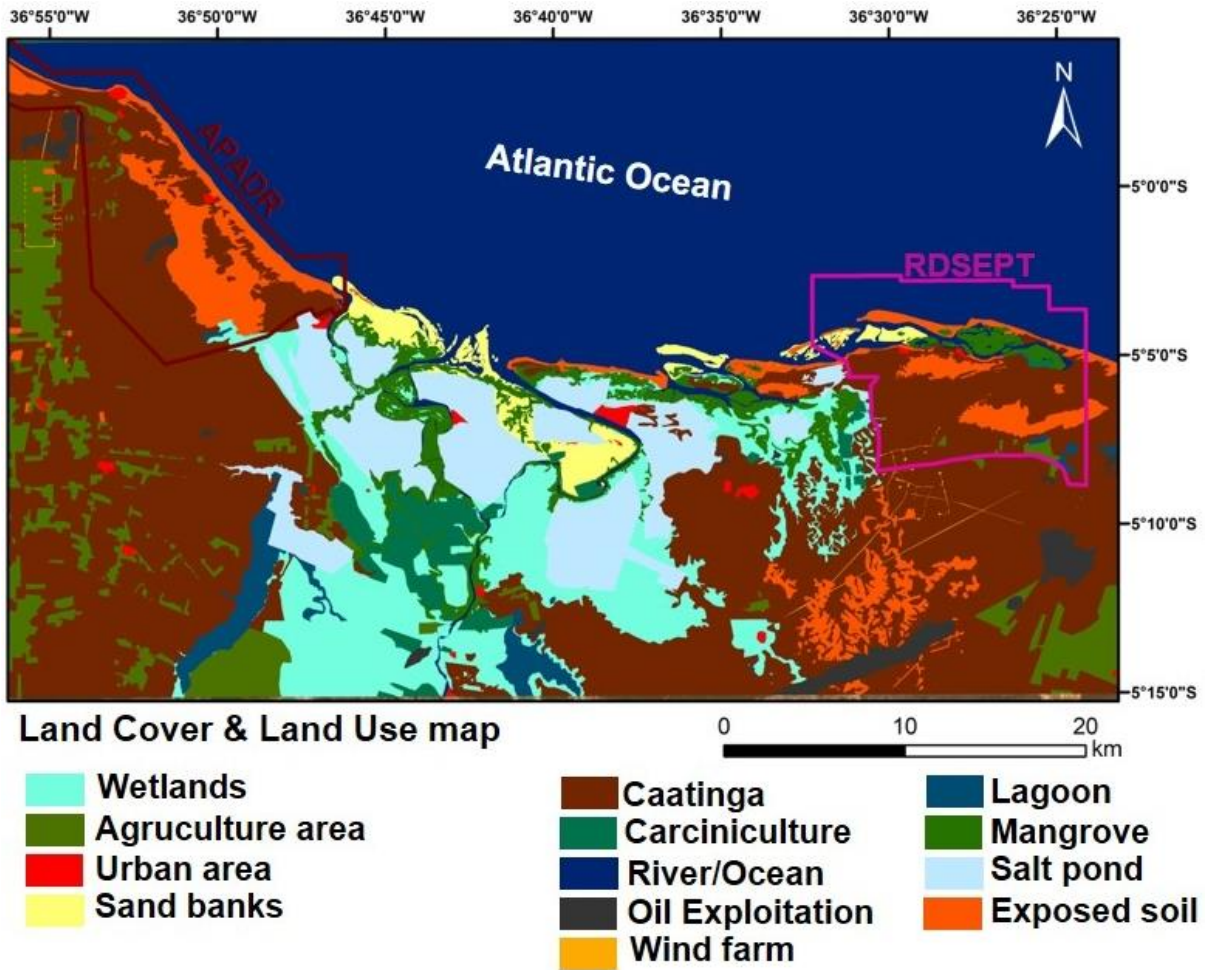
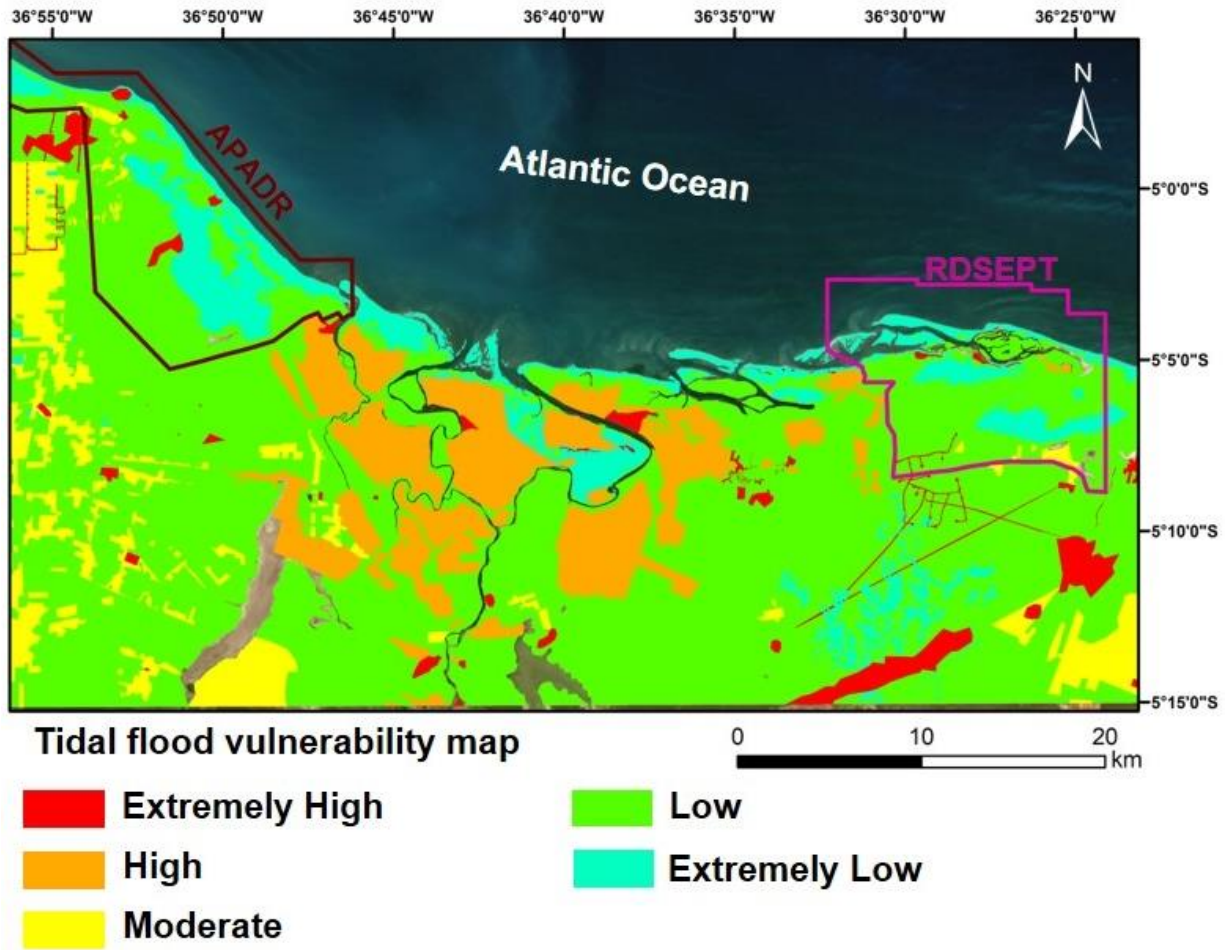


Figure 9: Land cover and land use map for study area.

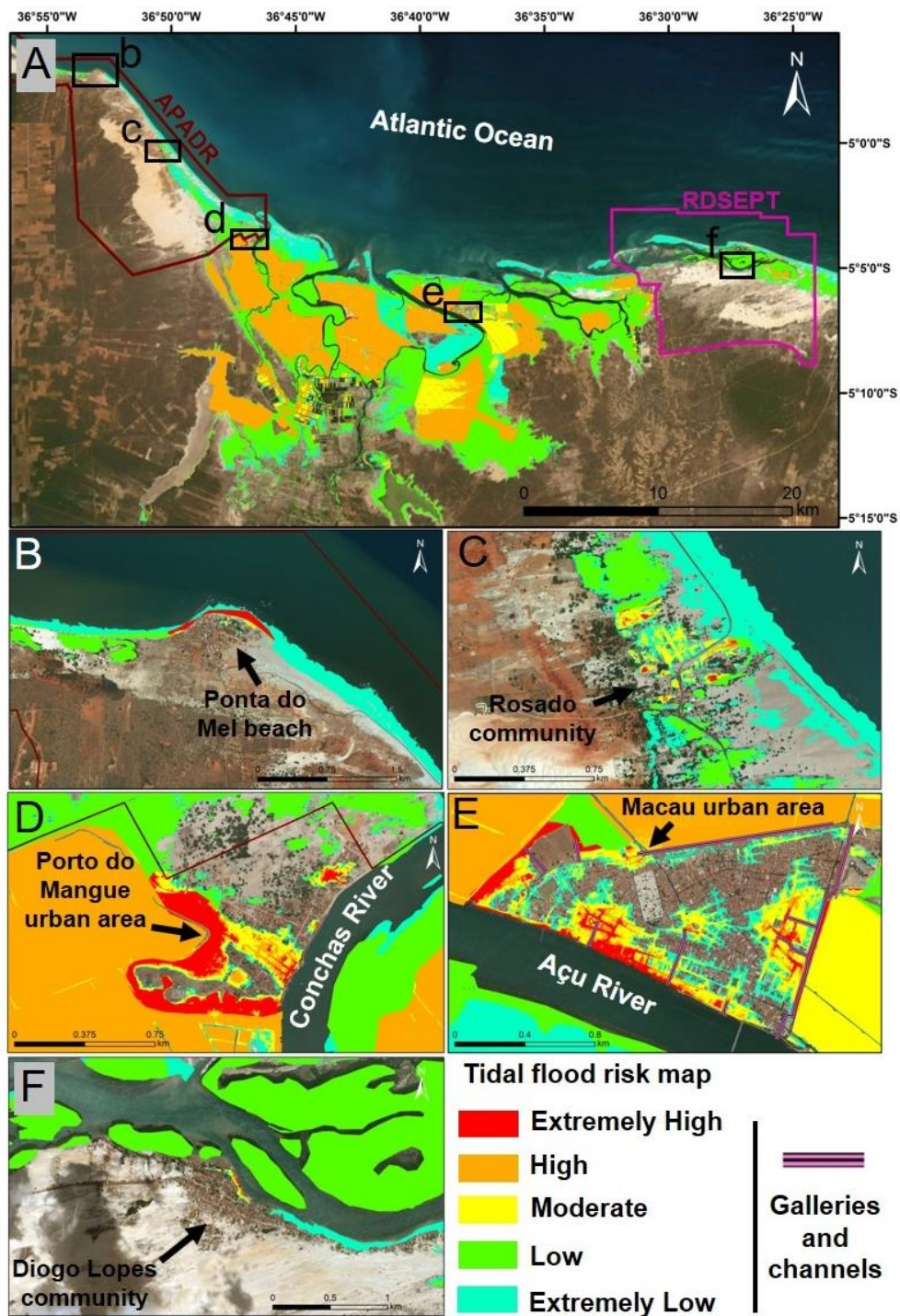


625

Figure 10: Tidal flood vulnerability map.

630





635 Figure 11: Tidal flood risk map for Piranhas Açú Estuary: (A) View of entire study area; (B) Ponta do Mel community; (C) Rosado community; (D) Porto do Mangue urban area; (E) Macau urban area; and (F) Diogo Lopes community. Basemap from ArcGIS Online: © ESRI.

**Table 1: Attributed value to hazard map.**

<b>Scenario</b>	<b>Value</b>	<b>Hazard</b>
Present	5	High
IBGE	4	Moderate
IPCC RCP 4.5	3	Low
IPCC RCP 8.5	1	Extremely Low

**Table 2: Attributed value to vulnerability map.**

<b>Category</b>	<b>Value</b>	<b>Vulnerability</b>
Urban area	5	Extremely High
Oil Exploitation	5	Extremely High
Wind farm	5	Extremely High
Shrimp farm	4	High
Salt pond	4	High
Agriculture area	3	Moderate
Wetlands	2	Low
Caatinga	2	Low
Mangrove	2	Low
Sand banks	1	Extremely Low
Exposed soil	1	Extremely Low
Lagoon	0	No vulnerability
River/Ocean	0	No vulnerability

640

**Table 3: Risk map value range.**

<b>Risk</b>	<b>Value Range</b>
Extremely High	$> 20$ and $\leq 25$
High	$> 15$ and $\leq 20$
Moderate	$> 10$ and $\leq 15$
Low	$> 5$ and $\leq 10$
Extremely Low	$> 0$ and $\leq 5$

**Table 4: Tidal flood quotas in the scenarios under study.**

<b>Hazard Class</b>	<b>Projection of MSL elevation to 2100 (m)</b>	<b>Meteorological tide (Tr20) (m)</b>	<b>Astronomical tide linked to SGB (Tr20) (m)</b>	<b>RMSE of DEM (m)</b>	<b>Flood quota (m)</b>
High	---	0.1590	1.7764	0.1704	<b>2.1058</b>
Moderate	0.1764	0.1590	1.7764	0.1704	<b>2.2822</b>
Low	0.5300	0.1590	1.7764	0.1704	<b>2.6358</b>
Extremely Low	0.7400	0.1590	1.7764	0.1704	<b>2.8458</b>

645 **Table 5: Area of land cover and land use categories.**

<b>Category</b>	<b>Area (km<sup>2</sup>)</b>	<b>Tidal Flood Vulnerability</b>	<b>Area (km<sup>2</sup>)</b>
Urban area	7.84		
Oil Explotation	27.37	Extremely High	40.17
Wind farm	4.96		
Shrimp farm	34.19		
Salt pond	130.94	High	165.13
Agriculture area	115.10	Moderate	115.10
Wetlands	174.74		
Caatinga	657.18	Low	883.84
Mangrove	51.91		
Sand banks	29.86		
Exposed soil	87.75	Extremely Low	117.61
Lagoon	24.22		
River/Ocean	848.97	No vulnerability	873.20

**Table 6: Area of Tidal Flood Risk in study area.**

<b>Tidal Flood Risk</b>	<b>Area (km<sup>2</sup>)</b>
Extremely High	0.53
High	117.76
Moderate	20.25
Low	135.23
Extremely Low	53.83
<b>Total</b>	<b>327.60</b>